Electronic Supplementary Material (ESI) for Physical Chemistry Chemical Physics.

Supplementary information for "Factors influencing hydrogen peroxide versus water inclusion in molecular crystals"

Ren A. Wiscons,[1] Rahul Nikhar,[2] Krzysztof Szalewicz*,[2] and Adam Matzger*[1]

[1]*Department of Chemistry and the Macromolecular Science and Engineering Program, 930 North University Ave, University of Michigan, Ann Arbor, Michigan 48109-1055, United States, E-mail: matzger@umich.edu*

[2]*Department of Physics and Astronomy, University of Delaware, Newark, Delaware 19716, E-mail: szalewic@udel.edu*

(Dated: April 1, 2022)

CONTENTS

I. EXPERIMENTAL METHODS

A. Cambridge Structural Database searching

Searching for hydrates in the Cambridge Structural Database (November 2018, v.5.40) was conducted using the IsoStar (2018, v2.3) program maintained by the Cambridge Crystallographic Data Centre. As IsoStar subdivides the hydrate crystal structures into bins for each contact group (functional group) based on degree of van der Waals overlap, the modal bin was selected for in-depth geometric analysis using the angle and torsion parameters specified for each functional group in Tables S1-S12. Hydrogen peroxide solvates were identified using the Substructure Search option available through ConQuest (v2.0.0). Given the uncertainty in identifying hydrogen atom positions by X-ray diffraction, interaction distances for each crystal structure were measured as the distances between the heteroatoms participating in the hydrogen bond. Interactions between crystallographically disordered molecules of water or hydrogen peroxide and functional groups of interest were not included in this analysis.

B. Analysis of experimentally determined crystal structures

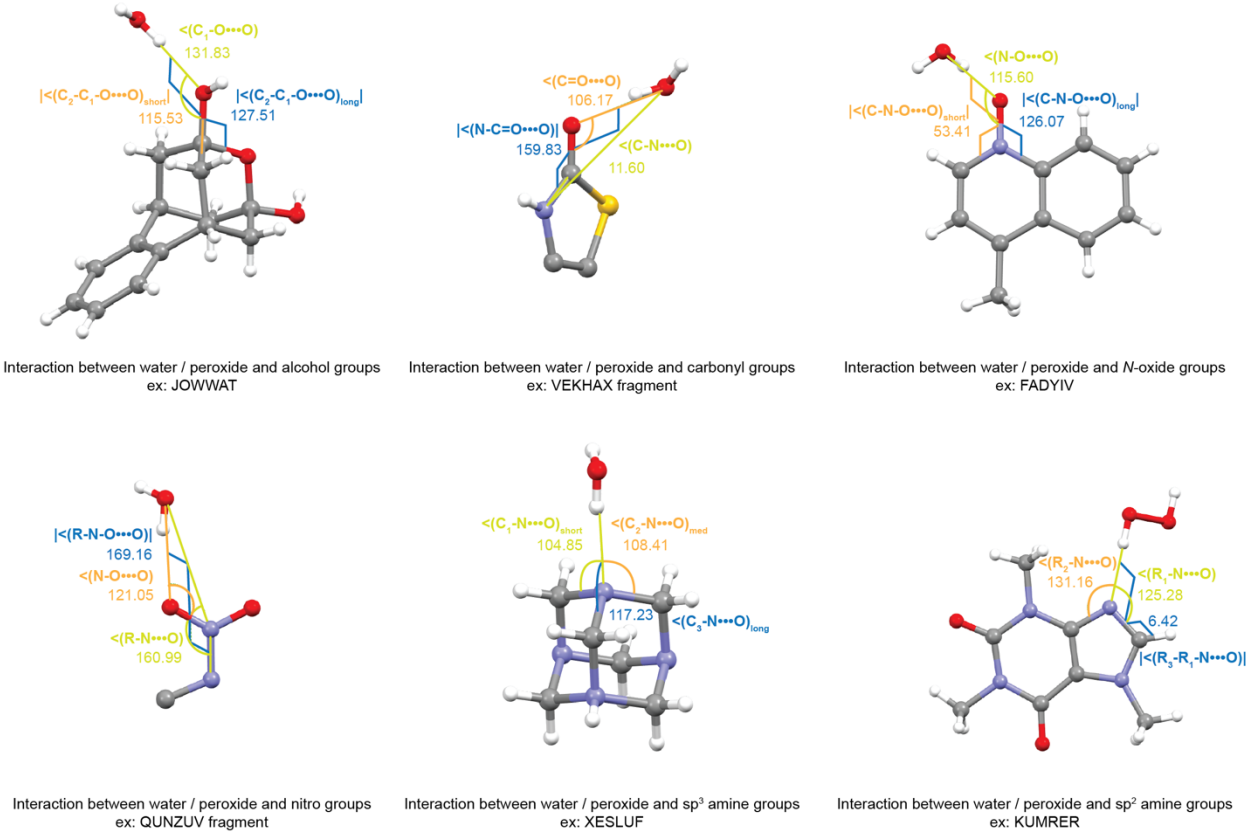

FIG. S1. Definition of geometric parameters and example crystal structures for measured interactions between water or hydrogen peroxide and various functional groups. All measured values presented in this figure represent dihedral or torsion angles given in degrees.

Figure S1 illustrates the angles measured for the six different types of interactions considered here using as examples actual crystals included in the tables. All angles are between heavy atoms. Most Y-X$\cdots$O angles are bond angles with $\cdots$ denoting the hydrogen bond. Two exceptions are C-N$\cdots$O angles in the carbonyl case and R-N$\cdots$O angle in the nitro case, where these are just angles between three atoms. If more than one X-Y$\cdots$O are measured, for example, the angles C_1-N$\cdots$O, C_2-N$\cdots$O, and C_3-N$\cdots$O in the case of sp^3 amines, we will use the subscript "short", "medium", and "long" to distinguish the angles, with the subscripts related to the lengths of C-N bonds. The subscripts n in C_n used in Fig. S1 are then redundant and will not be used in the tables. Similarly, the subscripts n in angles R_n-N$\cdots$O in the case of sp^2 amines in Fig. S1 are replaced by subscripts "short" and "long" in the tables. Similar rules apply to dihedral angles Z-Y-X$\cdots$O. If in most cases the X, Y, or Z atom is the same atom, we used this atom symbol in the tables. If several different atoms appear at these positions at different crystals, such positions are denoted by R. For example, the angle C_2-C_1-O$\cdots$O in the case of alcohol group is really the angle N-C-O$\cdots$O, but we will use symbol C since in most crystals C appears in the place of N. The sets of angles are in all cases redundant. For example, to determine the position of water's oxygen relative to the sp^3 amino group, if is sufficient to know angles C_1-N$\cdots$O and C_3-N$\cdots$O. For each particular crystal, the redundant angle is congruent with those of the minimal set. However, for the averages given in the tables, this is usually not true. The non-congruency is not large, e.g., for the sp^3 amino group it is within the standard deviations (given as values in parentheses in all tables). The choices of angles made in constructing the near-experimental dimer structures are described in Sec. III.

II. TABLES OF INTERACTION GEOMETRIES FOR FUNCTIONAL GROUPS FROM THE CSD SEARCH

A. Alcohol functional groups

TABLE S1. Refcodes and interaction parameters for the subset of crystal structures containing water$\cdots$alcohol interactions measured for this study where water is serving as a hydrogen bond acceptor.

Refcode	$\angle$(C-O$\cdots$O) (°)	$\lvert\angle(\mathrm{C-C-O\cdots O})_{\mathrm{short}}\rvert$ (°)	$\lvert\angle(\mathrm{C-C-O\cdots O})_{\mathrm{long}}\rvert$ (°)	d(O$\cdots$O) (Å)
ARARIV	96.15	60.90	179.08	2.767
ARARIV	100.21	60.10	179.87	2.823
BENDUU	119.59	63.42	173.46	2.766
BICVAN	108.18	65.90	171.84	2.822
CEZQUV	105.12	72.25	166.36	2.775
COSGUM	108.12	9.30	170.79	2.814
COWYAP	118.45	0.64	178.30	2.657
CUDVEE	123.65	115.17	130.03	2.757
DILMIW	126.72	101.62	137.94	2.969
EGINEP	117.36	71.43	175.59	2.746
JUBGEU	111.19	64.71	117.85	2.769
JUBGEU	98.22	75.89	168.10	2.854
MAWBIV	105.38	86.61	151.37	2.726
MELSUU	110.45	57.73	173.73	2.760
MELSUU	126.93	90.70	152.40	2.995
NURVOM	107.52	57.86	175.92	2.765
NURVOM	110.26	77.60	168.16	2.774
NURVOM	97.54	78.96	152.96	2.841
OLAZOQ	111.72	68.34	168.75	2.675
OLAZOQ	106.94	65.55	172.11	2.760
OPISOX	137.47	59.04	174.05	2.716
OPISOX	137.07	110.48	125.86	2.722
OPISOX	120.79	33.66	93.25	2.819
QIMJEB	122.76	105.33	133.58	2.980
QIMJEB	124.54	9.17	133.92	2.991
SUPVUW	131.51	59.99	173.67	2.809
XEJMAA	101.25	84.69	155.37	2.734
XEJMAA	123.85	79.42	161.90	2.898
Average	120(10)	70(30)	160(20)	2.80(2)

Number of Structures: 18
Number of Interactions: 28

TABLE S2. Refcodes and interaction parameters for the subset of crystal structures containing water$\cdots$alcohol interactions measured for this study where water is serving as a hydrogen bond donor.

Refcode	$\angle$(C-O$\cdots$O) (°)	$\lvert\angle(\mathrm{C-C-O\cdots O})_{\mathrm{short}}\rvert$ (°)	$\lvert\angle(\mathrm{C-C-O\cdots O})_{\mathrm{long}}\rvert$ (°)	d(O$\cdots$O) (Å)
ACLACT	103.52	82.91	155.97	2.794
ACLACT	118.02	97.25	134.23	2.898
ACOQEP	129.26	76.31	167.83	2.741
AXUKAH	121.15	74.80	165.15	2.806
BIGWET	122.45	86.97	156.61	2.820
BIGWET	123.84	116.70	119.10	2.830
BIKCIH10	125.50	120.74	122.38	2.799
BODGEG	111.99	69.97	165.44	2.768
CAMTIU	118.47	70.71	163.78	2.775
CAMTIU	129.36	95.29	144.95	2.815
CEQJEO	142.38	85.44	153.04	2.714
CEQJEO	125.33	101.29	138.84	2.876
CIDRUC	121.25	65.93	173.39	2.757
CUPSAI	112.92	73.21	165.60	2.801
CUQGIE	124.18	111.02	127.57	2.682
CUQGIE	98.18	92.92	146.86	2.759
CUQGIE	131.66	103.77	134.59	2.764
CUQGIE	132.23	116.76	121.69	2.765
DEZHOG	114.91	11.26	168.73	2.628
DEZHOG	118.05	38.06	143.21	2.790
DIDDUQ	111.04	109.47	130.49	2.796
DUWKUD	105.40	16.29	133.62	2.763
DXIFPO	134.30	98.82	136.90	2.776
ELEVOG	113.82	60.33	179.68	2.779
JOWWAT	125.33	92.32	150.17	2.772
JOWWAT	131.83	115.53	127.51	2.804
KEPYUB	147.56	115.84	120.41	2.758
MOPMOT	113.41	79.39	159.47	2.773
MUSPAT	119.74	67.79	176.98	2.760
OFOQAD	115.57	101.20	137.46	2.697
OWOSOK	116.77	84.08	153.32	2.759
PEMTOT	105.37	110.53	129.49	2.744
RIWCIK	132.82	132.82	139.52	2.798
SOBJID	154.53	106.98	132.13	2.776
Average	120(10)	90(30)	150(20)	2.775(2)

Number of Structures: 25
Number of Interactions: 34

TABLE S3. Refcodes and interaction parameters for the subset of crystal structures containing hydrogen peroxide$\cdots$alcohol interactions measured for this study.

Refcode	$\angle$(C-O$\cdots$O) (°)	$\lvert\angle(\mathrm{C-C-O\cdots O})_{\mathrm{short}}\rvert$ (°)	$\lvert\angle(\mathrm{C-C-O\cdots O})_{\mathrm{long}}\rvert$ (°)	d(O$\cdots$O) (Å)
KULMOU	105.25	109.00	130.06	2.692
TANCOC	134.88	71.60	170.66	2.681
TANCUI	100.10	69.85	108.90	2.963
UDUWEX	105.06	109.07	129.92	2.683
Average	110(20)	90(20)	140(30)	2.75(8)

Number of Structures: 4
Number of Interactions: 4

B. Carbonyl functional groups

TABLE S4. Refcodes and interaction parameters for the subset of crystal structures containing water$\cdots$carbonyl (amide) interactions measured for this study.

Refcode	$\angle$(C-N$\cdots$O) (°)	$\angle$(C=O$\cdots$O) (°)	$\lvert\angle$(N $-$ C = O$\cdots$O)$\rvert$ (°)	d(O$\cdots$O) (Å)
AKEYAQ	38.64	136.86	110.40	2.830
AKEYAQ	24.37	110.88	139.51	2.831
AKEYAQ	62.40	110.24	71.68	2.851
ALUREF	23.04	126.37	147.09	2.810
ASOTEJ	21.74	145.14	172.55	2.748
CAMVES02	19.93	125.32	152.57	2.719
CAMVES02	15.28	106.27	154.46	2.830
CISWOQ01	64.61	135.27	29.92	2.839
ECECEU	27.63	115.69	133.49	2.781
ECECEU	29.71	130.35	132.61	2.793
EWIJIF	24.64	134.15	150.36	2.820
FUBXUX	39.17	151.21	111.14	2.848
FUMNEI	7.70	116.90	170.48	2.786
GESKUK	38.14	137.25	113.55	2.818
GEWWAG	63.54	131.56	52.99	2.800
GEWWAG	18.42	132.99	175.77	2.832
GITGUM	74.16	119.58	9.16	2.795
GUHMIG	35.33	123.38	115.87	2.819
HAVZEL	20.72	134.94	150.20	2.829
HAVZEL	54.78	138.94	54.11	2.813
MUXHIX	11.74	116.51	170.54	2.703
VEKHAX	11.60	106.17	159.83	2.882
Average	30(20)	130(10)	120(50)	2.808(9)

Number of Structures: 16
Number of Interactions: 22

TABLE S5. Refcodes and interaction parameters for the subset of crystal structures containing hydrogen peroxide$\cdots$carbonyl (amide) interactions measured for this study.

Refcode	$\angle$(C-N$\cdots$O) (°)	$\angle$(C=O$\cdots$O) (°)	$\lvert\angle$(N $-$ C = O$\cdots$O)$\rvert$ (°)	d(O$\cdots$O) (Å)
KELXEH	46.59	149.00	83.33	2.765
YAFGEU	24.51	133.00	155.32	2.673
Average	40(20)	140(10)	120(50)	2.72(5)

Number of Structures: 2
Number of Interactions: 2

C. N-oxide functional groups

TABLE S6. Refcodes and interaction parameters for the subset of crystal structures containing water$\cdots$*N*-oxide (aliphatic and aromatic) interactions measured for this study.

Refcode	$\angle$(N-O$\cdots$O) (°)	$\lvert\angle(\mathrm{C-N-O\cdots O})_{\mathrm{short}}\rvert$ (°)	$\lvert\angle(\mathrm{C-N-O\cdots O})_{\mathrm{long}}\rvert$ (°)	d(O$\cdots$O) (Å)
ACOHAC	110.62	94.63	85.48	2.787
AHITAO	116.16	41.36	138.49	2.782
AHITES	137.68	8.31	169.76	2.756
AHOVAW	126.80	69.52	111.49	2.663
AHOVAW	130.98	14.97	164.97	2.702
AHOVAW	120.25	4.22	174.77	2.710
AHOVAW	121.32	80.14	101.67	2.753
AHOVAW	118.35	13.14	165.05	2.784
AQOPAZ	107.44	63.25	116.23	2.786
BAFVUZ	135.03	91.39	91.39	2.683
BILJUD	112.59	62.12	116.71	2.774
BILJUD01	108.97	47.93	132.91	2.715
BILJUD01	112.49	60.60	118.56	2.767
CIWDIX	141.41	55.19	124.54	2.749
CIWDIX	122.00	86.76	93.51	2.756
COKBUZ	109.74	33.20	148.30	2.766
COKBUZ	116.44	88.42	90.07	2.772
COKBUZ	126.12	43.14	138.36	2.787
DATHIQ	121.56	104.40	136.69	2.634
DATHIQ	113.39	70.08	168.38	2.659
EVIKOJ	112.36	49.88	129.35	2.741
EVIKOJ	115.03	40.41	143.77	2.753
EYUBUX	113.36	86.93	93.58	2.787
EYUBUX	110.41	20.85	158.64	2.805
FADYAN	112.79	80.72	98.71	2.836
FADYIV	113.04	50.06	130.46	2.778
FADYIV	115.06	53.41	126.07	2.797
FOGTOL	119.76	23.07	155.00	2.834
FURFIH	120.76	68.43	170.67	2.740
FURFIH	114.31	69.24	172.20	2.646
GAKSAM	113.98	67.76	112.30	2.731
GAKSAM	113.07	70.68	109.26	2.740
HUVLOB	98.17	58.62	121.58	2.816
ITEWOT	110.04	49.85	128.77	2.727
ITEWOT	141.75	43.48	137.91	2.800
KECZIC	122.00	65.78	114.24	2.740
KECZIC	121.82	75.11	104.87	2.757
KECZOI	129.28	65.98	114.40	2.762
KECZOI	120.32	77.30	102.33	2.764
Average	119(9)	60(30)	130(30)	2.752(2)

Number of Structures: 22
Number of Interactions: 39

TABLE S7. Refcodes and interaction parameters for the subset of crystal structures containing hydrogen peroxide$\cdots$*N*-oxide (aliphatic and aromatic) interactions measured for this study.

Refcode	$\angle$(N-O$\cdots$O) (°)	$\lvert\angle(\mathrm{C-N-O\cdots O})_{\mathrm{short}}\rvert$ (°)	$\lvert\angle(\mathrm{C-N-O\cdots O})_{\mathrm{long}}\rvert$ (°)	d(O$\cdots$O) (Å)
JELQOJ	126.22	99.19	77.19	2.681
JELQOJ	117.85	48.49	135.12	2.707
JESXEN	118.52	37.90	143.53	2.672
KELXEH	138.91	65.30	177.69	2.694
Average	125(9)	70(20)	140(40)	2.70(1)

Number of Structures: 3
Number of Interactions: 5

D. Nitro functional groups

TABLE S8. Refcodes and interaction parameters for the subset of crystal structures containing water$\cdots$nitro interactions measured for this study.

Refcode	$\angle$(R-N$\cdots$O) (°)	$\angle$(N-O$\cdots$O) (°)	$\lvert\angle$(R $-$ N $-$ O$\cdots$O)$\rvert$ (°)	d(O$\cdots$N) (Å)
CIMQOG	128.65	151.50	125.22	2.866
FULTUC	169.05	109.65	177.01	2.894
FULTUC	135.30	154.15	161.18	2.863
FULTUC	160.12	111.47	160.25	2.978
GEPBOV	92.38	141.32	10.82	2.901
HODHUE	155.50	105.50	149.97	2.868
LOXVEZ	143.03	117.08	137.33	2.908
LOXVEZ	163.55	107.71	163.17	2.916
MEDDIL	134.11	121.60	127.56	2.865
MUGLEH	152.86	114.72	154.52	2.865
QUNZUV	160.99	121.05	169.16	2.892
SOQNOC	176.56	103.49	176.22	2.895
SOQNOC	70.81	110.87	27.46	2.837
XUZBAW	135.95	115.39	128.11	2.894
Average	140(30)	120(20)	130(50)	2.889(9)

Number of Structures: 10
Number of Interactions: 14

E. sp^3 nitrogen functional groups

TABLE S9. Refcodes and interaction parameters for the subset of crystal structures containing water$\cdots$amine interactions measured for this study.

Refcode	$\angle$(C-N$\cdots$O)$_{\text{short}}$ (°)	$\angle$(C-N$\cdots$O)$_{\text{med}}$ (°)	$\angle$(C-N$\cdots$O)$_{\text{long}}$ (°)	d(O$\cdots$N) (Å)
AFUREA	91.94	109.17	124.33	2.892
CAFGIB	92.61	102.08	126.93	2.904
CIWJOH01	103.12	103.14	125.63	2.877
CIWJOH10	102.47	109.37	120.04	2.808
COBZID	96.85	109.43	111.94	2.85
DILMAM	102.17	107.77	113.67	2.902
FAKKAF	96.27	106.08	125.25	2.891
FOMQOO	101.26	102.48	127.53	2.892
KEYXOB	96.24	102.25	127.72	2.909
LAXSAG	91.14	106.11	122.94	2.968
LAXSAG	102.24	108.90	115.64	2.928
MEZBUR	90.14	109.86	124.07	2.927
NDNCLH01	95.09	111.90	119.37	2.889
PEPCIW	104.63	109.53	113.04	2.931
QOHYAO01	107.92	108.73	115.45	2.934
QOHYAO01	107.62	109.55	114.87	2.928
QOHYAO01	107.92	108.73	115.45	2.934
ROZVUY	83.70	99.09	116.99	2.912
TEBDIP	95.99	107.31	122.79	2.918
TIKPIN	92.39	105.26	113.58	2.922
TOZNOL	102.16	111.80	114.30	2.915
WAYZUT	94.31	101.65	130.07	2.881
XALNUU	96.29	99.45	111.74	2.907
XESLUF	104.85	108.41	117.23	2.921
YUJNUM01	104.59	105.36	116.28	2.928
YUJNUM02	105.08	105.65	116.93	2.947
Average	99(6)	107(4)	119(6)	2.908(6)

Number of Structures: 22
Number of Interactions: 26

TABLE S10. Refcodes and interaction parameters for the subset of crystal structures containing hydrogen peroxide$\cdots$amine interactions measured for this study.

Refcode	$\angle$(C-N$\cdots$O)$_{\text{short}}$ (°)	$\angle$(C-N$\cdots$O)$_{\text{med}}$ (°)	$\angle$(C-N$\cdots$O)$_{\text{long}}$ (°)	d(O$\cdots$N) (Å)
MUXHIX	96.07	116.04	125.6	2.887
QOHXUH	108.39	109.33	113.05	2.659
VAYGUY	107.97	108.41	109.99	2.782
Average	104(7)	111(4)	116(8)	2.78(7)

Number of Structures: 3
Number of Interactions: 3

F. sp^2 nitrogen functional groups

TABLE S11. Refcodes and interaction parameters for the subset of crystal structures containing water$\cdots$aromatic nitrogen interactions measured for this study.

Refcode	$\angle$(R-N$\cdots$O)$_{\text{short}}$ (°)	$\angle$(R-N$\cdots$O)$_{\text{long}}$ (°)	$\lvert\angle$(R $-$ R $-$ N$\cdots$O)$\rvert$ (°)	d(O$\cdots$N) (Å)
BULZOY	97.71	149.05	13.29	2.897
BUTGAZ01	113.57	129.59	1.39	2.917
CEQLUI	106.47	143.47		2.828
DABWOU	125.79	126.21	9.74	2.907
EJUWIR	91.60	151.82	4.49	2.849
FOXJIN	128.95	130.56	9.94	2.871
GIJREY	104.11	130.02	29.83	2.907
HENGIT	115.93	134.48	23.47	2.881
HOSVES	107.27	142.32	21.83	2.904
JUVYUW	107.27	140.79	33.13	2.793
JUVYUW	105.26	143.25	30.60	2.900
KIDHAJ	116.50	119.60	2.80	2.936
LODPAX	112.62	138.70	8.00	2.871
LUZFUJ	118.11	126.24		2.930
MILMEZ	115.04	136.13	14.33	2.871
NOQZID	124.01	131.57	2.58	2.929
PIVVUM	107.05	131.83	20.89	2.909
PORXOL	93.27	146.63	12.83	2.899
POVLUJ	116.90	129.64		2.910
PUVQIG01	116.08	138.77	9.67	2.870
QEKMIF	121.06	123.69	0.84	2.933
QILFIA	112.36	135.20	15.95	2.889
QUJHOT	109.49	133.44	7.88	2.829
RELCIV	111.38	117.09	47.94	2.828
RIQREO	103.85	136.56	8.17	2.821
RUVDUI	114.01	128.30	31.56	2.910
Average	111(9)	134(9)	10(10)	2.884(8)

Number of Structures: 25
Number of Interactions: 26

TABLE S12. Refcodes and interaction parameters for the subset of crystal structures containing hydrogen peroxide$\cdots$aromatic nitrogen interactions measured for this study.

Refcode	$\angle$(R-N$\cdots$O)$_{\text{short}}$ (°)	$\angle$(R-N$\cdots$O)$_{\text{long}}$ (°)	$\lvert\angle(\text{R}-\text{R}-\text{N}\cdots\text{O})\rvert$ (°)	d(O$\cdots$N) (Å)
DOJMIZ	118.20	136.67	1.83	2.703
KUMRER	125.28	131.16	6.42	2.913
SEMXIU	116.87	122.73	20.42	2.737
UDUROD	116.02	130.30	27.81	2.732
UDUROD	116.21	131.18	33.90	2.750
YAFFUJ	121.07	123.98	3.02	2.721
Average	119(4)	129(5)	20(10)	2.76(3)

Number of Structures: 5
Number of Interactions: 6

G. Summary tables of functional group averages and deviations

TABLE S13. Average interaction distances and angles between oxygen-containing hydrogen bond accepting functional groups and water or hydrogen peroxide. The numbers in parentheses are the standard deviations for the data sets analyzed to calculate the averages.

O-H$\cdots$O-H (Alcohol)	d(O$\cdots$O)	$\angle$(C-O$\cdots$O)	$\lvert\angle(\mathrm{C-C-O\cdots O})_{\mathrm{short}}\rvert$	$\lvert\angle(\mathrm{C-C-O\cdots O})_{\mathrm{long}}\rvert$
H_2O Average of Bin Mode	2.775(2)	120(10)	90(30)	150(20)
H_2O_2 Average of CSD	2.75(8)	110(20)	90(20)	140(30)
O-H$\cdots$O=C (Amide)	d(O$\cdots$O)	$\angle$(C-N$\cdots$O)	$\angle$(C=O$\cdots$O)	$\lvert\angle(\mathrm{N-C=O\cdots O})\rvert$
H_2O Average of CSD Organics	2.808(9)	30(20)	130(10)	120(50)
H_2O_2 Average of CSD (COO)	2.72(5)	40(20)	140(10)	120(50)
O-H$\cdots$O-N (N-oxide)	d(O$\cdots$O)	$\angle$(N-O$\cdots$O)	$\lvert\angle(\mathrm{C-N-O\cdots O})_{\mathrm{short}}\rvert$	$\lvert\angle(\mathrm{C-N-O\cdots O})_{\mathrm{long}}\rvert$
H_2O Average of Bin Mode	2.752(2)	119(9)	60(30)	130(30)
H_2O_2 Average of CSD	2.70(1)	125(9)	70(20)	140(40)
O-H$\cdots$O$_2$-N (Nitro)	d(O$\cdots$O)	$\angle$(R-N$\cdots$O)	$\angle$(N-O$\cdots$O)	$\lvert\angle(\mathrm{R-N-O\cdots O})\rvert$
H_2O Average of Bin Mode	2.889(9)	140(30)	120(20)	130(50)
H_2O_2 Refcode: AZACIP	3.037	152.02	127.95	167.69

TABLE S14. Average interaction distances and angles between nitrogen-containing hydrogen bond accepting functional groups and water or hydrogen peroxide. The numbers in parentheses are the standard deviations for the data sets analyzed to calculate the averages.

O-H$\cdots$N (sp^3)	d(O$\cdots$N)	$\angle(\mathrm{C-N\cdots O})_{\mathrm{short}}$	$\angle(\mathrm{C-N\cdots O})_{\mathrm{med}}$	$\angle(\mathrm{C-N\cdots O})_{\mathrm{long}}$
H_2O Average of Bin Mode	2.908(6)	99(6)	107(4)	119(6)
H_2O_2 Average of CSD	2.78(7)	104(7)	111(4)	116(8)
O-H$\cdots$N (sp^2)	d(O$\cdots$N)	$\angle(\mathrm{R-N\cdots O})_{\mathrm{short}}$	$\angle(\mathrm{R-N\cdots O})_{\mathrm{long}}$	$\lvert\angle(\mathrm{R-R-N\cdots O})\rvert$
H_2O Average of CSD Organics	2.884(8)	111(9)	134(9)	10(10)
H_2O_2 Average of CSD	2.76(3)	119(4)	129(5)	20(10)

III. NEAR-EXPERIMENTAL DIMER CONFIGURATIONS

The coordinates of oxygen atoms in water or hydrogen peroxide were fixed with respect to model molecules by using the distance, a bond angle, and a dihedral angle given in Tables S13 and S14. For all dimers, except the ones involving sp^3 nitrogen, the redundant angles that were not used are: $|\angle(\mathrm{C}-\mathrm{C}-\mathrm{O}\cdots\mathrm{O})_{\mathrm{short}}|$, $\angle$(C-N$\cdots$O), $|\angle(\mathrm{C}-\mathrm{N}-\mathrm{O}\cdots\mathrm{O})_{\mathrm{short}}|$, $\angle(\mathrm{R}-\mathrm{N}\cdots\mathrm{O})$, and $\angle$(R-N$\cdots$O)$_{\mathrm{long}}$ in alcohol, carbonyl, N-oxide, nitro, and sp^2 nitrogen cases, respectively. The redundant angles were not used, but we checked that their values in the model systems are within the standard deviation given in Tables S13 and S14. In case of the sp^3 nitrogen, we have kept the $\angle$(C-N$\cdots$O)$_{\mathrm{long}}$ angle at its averaged experimental value and rotated the N$\cdots$O hydrogen bond until the two other angles had values within the experimental uncertainties. The values of these angles used in our calculations are 94° (106°) for $\angle$(H-N$\cdots$O)$_{\mathrm{short}}$ and 111° (108°) for $\angle$(H-N$\cdots$O)$_{\mathrm{med}}$ for the water (hydrogen peroxide) dimer. In case of alcohol functional group, the leftmost carbon atoms in the dihedral angles $|\angle(\mathrm{C}-\mathrm{C}-\mathrm{O}\cdots\mathrm{O})_{\mathrm{short}}|$ and $|\angle(\mathrm{C}-\mathrm{C}-\mathrm{O}\cdots\mathrm{O})_{\mathrm{long}}|$ were replaced by hydrogens bonded to the carbon in methanol. Similarly, in case of sp^3 nitrogen functional group, the carbon atoms in the angles $\angle$(C-N$\cdots$O)$_{\mathrm{short}}$ and $\angle$(C-N$\cdots$O)$_{\mathrm{med}}$ were replaced by hydrogens bonded to the nitrogen in methylamine. After the position of the oxygen atom was established, the orientation of water or hydrogen peroxide was found by minimizing the interaction energies given by the appropriate PES with respect to the rotation around space-fixed x, y, and z axes to get near-experimental dimer configurations.

IV. GENERATION OF POTENTIAL ENERGY SURFACES AND FIRST-PRINCIPLES METHODOLOGY

The autoPES software package [1] was used to generate potential energy surfaces for the dimers under consideration. Monomers were assumed rigid in all calculations. The process is divided into five parts: asymptotic calculations, generation of grid points of close-range dimer configurations, calculation of interaction energies at close-range grid points, fitting an analytic functional form to the data, and finally evaluation of the quality of the fit and iterative improvement. Each step is described in detail in Ref. 1. A brief outline is given below. The overall computational cost and the number of close-range grid points are reduced by using asymptotic calculations. Asymptotic expansion is used in the region where the charge overlap effects can be neglected, which is about 1.5 times the radial van der Waals minimum intermonomer separation for a given orientation. Multipole expansion located at the center of mass (COM) of monomers [2, 3] is used to calculate the interaction energy of the dimers at asymptotic separations. The coefficients of the expansion are computed from monomer's charge distributions and static and frequency-dependent density susceptibilities (FDDS). In order to connect seamlessly with the close-range calculations, the same basis set and level of theory is used for calculating monomer properties as in the close-range calculations. A set of 12,000 dimer grid points was used for calculating interaction energies in the asymptotic region. A guided Monte Carlo procedure was used for generating close-range grid points, with higher concentration of grid points in energetically relevant regions such as minima. The interaction energy at each of these close-range points was computed using the SAPT(DFT) method at the level specified in the main text. A set of six coordinates, the distance between the monomer's COMs and five Euler angles describing the relative angular orientation of the monomers, are used to describe the grid points. However, the functional form of the fit uses only atom-atom distances r_{ab} where atom $a(b)$ belongs to monomer A(B). After calculating interaction energies in the asymptotic and close-range regions, the energies are fit with the following functional form of the potential:

$$V = V_{\text{elst}}+V_{\text{exp}}+V^{(2)}_{\text{asymp}} = \sum_{a\in A, b\in B} u_{ab}(r_{ab}) = \sum_{a\in A, b\in B} \left[u_{\text{elst},ab}(r_{ab}) + u_{\text{exp},ab}(r_{ab}) + u^{(2)}_{\text{asymp},ab}(r_{ab})\right] \tag{1}$$

The atom-atom functions are of the form

$$\begin{aligned} u_{\text{elst},ab}(r_{ab}) =& f_1(\delta^{ab}_1, r_{ab})\frac{q_a q_b}{r_{ab}} \\ u_{\text{exp},ab}(r_{ab}) =& \left[1 + \sum_{i=1}^{2} a^{ab}_i (r_{ab})^i\right] e^{\alpha^{ab}-\beta^{ab} r_{ab}} + \frac{A^{ab}_{12}}{(r_{ab})^{12}} \\ u^{(2)}_{\text{asymp},ab}(r_{ab}) =& -\sum_{n=6,8} f_n(\delta^{ab}_n, r_{ab})\frac{C^{ab}_n}{(r_{ab})^n}, \end{aligned} \tag{2}$$

where f_n are Tang-Toennies damping functions [4]

$$f_n(\delta^{ab}_n, r_{ab}) = 1 - e^{-\delta r}\sum_{m=0}^{n}\frac{(\delta r)^m}{m!}. \tag{3}$$

The distributed induction plus dispersion coefficients C_n^{ab} and the partial charges q_x were fit to the asymptotic-expansion COM-COM interaction energies at long-range grid points. These are kept unchanged in the subsequent fitting stage in order to make sure the PES behaves correctly in the asymptotic region. The remaining parameters: α^{ab}, β^{ab}, δ_n^{ab}, a_i^{ab}, and A_{12}^{ab}, were fit to energies calculated at short-range grid points. To ensure correct repulsive behavior at very close range, coefficients A_{12}^{ab} are constrained to be positive. Geometric combination rule is used for C_n^{ab} parameters such that C_n^{ab} is expressed through the atomic parameters C_n^a and C_n^b. Similarly, arithmetic combination rule is used for parameters α^{ab} and β^{ab}. For details of this fitting stage, see Ref. 1, Sec. VI. The quality of the PES was evaluated after the fitting stage using two criteria, and additional iterations were performed if necessary. The first criterion ensures correct repulsive behavior such that there are no 'holes' in the PES at very-close range. If holes are found then additional grid points are added at appropriate configurations, and the potential is refit. The procedure is repeated until there is a barrier of at least 15 kcal/mol for each orientation of the monomer. The second criterion evaluates the accuracy of the PES by comparing the root mean square error (RMSE) of the 85% of the total grid points called the fitting (training) set with the remaining 15% of the total grid points called the test set. If the RMSE of the test set is greater by a factor of 1.2 than that of the fitting set, then a PES is considered to be not converged. Additional grid points are added at close-range and the procedure is repeated until the above two criteria are satisfied. In the final fitting stage, the test set was not used and the PES was fit to all the available data.

The interaction energies were computed using symmetry adapted perturbation theory (SAPT)[3] based on density functional theory (DFT) description of monomers, denoted as SAPT(DFT) and developed in Refs. 5–13, in the density fitting version [9, 14, 15]. The ORCA[16, 17] electronic structure package was used for performing monomer DFT calculations with the PBE functional[18] including the gradient-regulated asymptotic correction (GRAC)[19, 20]. The ionization potential of each monomer, required for GRAC, was computed using separate DFT calculations with the PBE functional. The augmented correlation-consistent double-zeta (aug-cc-pVDZ) basis set[21] together with the corresponding correlation-energy fitted auxiliary bases from Ref. 22 were used in all cases. We have applied the monomer-centered 'plus' basis set (MC^+BS) form with midbond functions, see Ref. 23. Midbond function exponents and placement are as described in Ref. 24, with the midbond auxiliary basis set from Ref. 15. The SAPT2016 system of codes [25] was used in calculations. For all dimers, the $\delta E^{\rm HF}_{\rm int,resp}$ correction [26, 27], which accounts mostly for induction and exchange-induction effects beyond second order, was added to the SAPT(DFT) interaction energy, see the main text. The accuracy of the SAPT(DFT) interaction energies for most systems increases by including $\delta E^{\rm HF}_{\rm int,resp}$ terms, but its use increases the associated computational cost by about 60%. Based on the magnitude of the electric dipole moments of the monomers and the induction component of the interaction energy, autoPES determines if $\delta E^{\rm HF}_{\rm int,resp}$ should be included for a given dimer, see Ref. 1. $E^{(2)}_{\rm ind}$ was computed from coupled Kohn Sham (CKS) FDDSs at zero frequency. The exchange-induction energy, $E^{(2)}_{\rm exch-ind}$, was also computed at the CKS level, i.e., from the CKS FDDS amplitudes. The dispersion energy, $E^{(2)}_{\rm disp}$, was computed from frequency-dependent CKS FDDSs. Fast dispersion method, developed in Ref. 28, was used to compute this term. When this approach is used, the exchange counterpart, $E^{(2)}_{\rm exch-disp}$, can be computed only in the uncoupled form. It was then scaled to approximate the CKS value as described in Ref. 12.

The $V_{\rm elst}$ term in Eq. (1) was fitted to the asymptotic values of $E^{(1)}_{\rm elst}$, and was damped

(using close-range values of $E^{(1)}_{\rm elst}$) to ensure correct behavior of this component at short-ranges. The coefficients C^{ab}_n in $V^{(2)}_{\rm asymp}$ were fit to the sum of the COM-COM asymptotic expansions of $E^{(2)}_{\rm ind}$ and $E^{(2)}_{\rm disp}$. The damping factors were fit to $E_{\rm indx} + E^{(2)}_{\rm dispx}$ computed at close range. Finally, the exponential term, $V_{\rm exp}$, was fit to $E_{\rm int} - V_{\rm elst} - V^{(2)}_{\rm asym}$. It mainly reproduces the sum of exchange components of $E_{\rm int}$.

V. SAPT COMPONENTS AT GLOBAL MINIMA OF PESS FOR WATER AND HYDROGEN PEROXIDE INTERACTING WITH MODEL MOLECULES

The global energy minimum geometries for each heterodimer interaction are presented in Figure 2 of the main text, while Figure S2 displays interaction energies, hydrogen bond distances, and SAPT components. In general, the small molecules considered were found

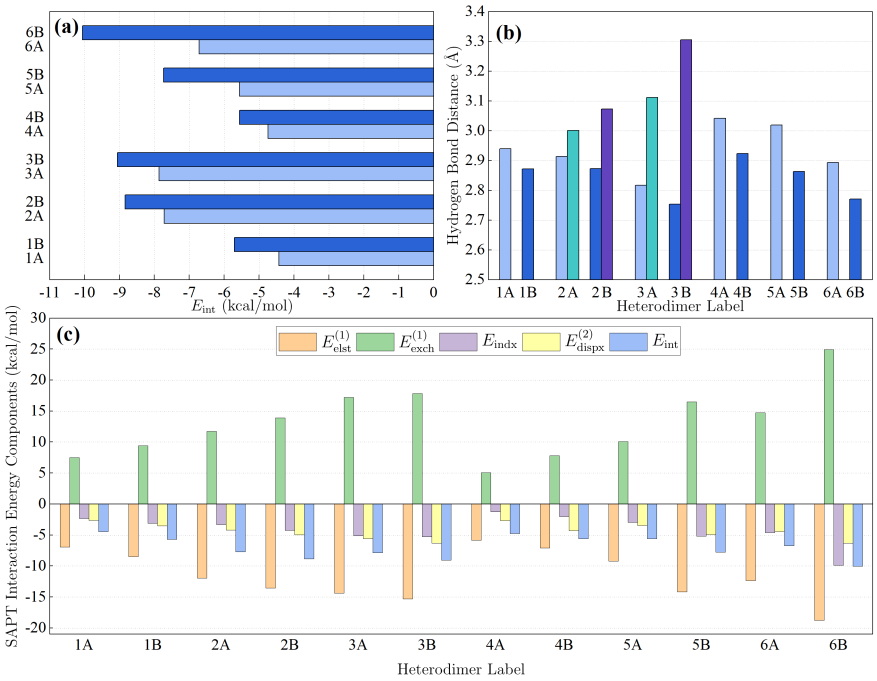

FIG. S2. (a) Interaction energy comparison for model molecules interacting with water or hydrogen peroxide at the global minima of the PESs. Top to bottom: water and hydrogen peroxide dimers of imidazole, methylamine, nitromethane, pyridine-N-oxide, formamide, and methanol; (b) hydrogen bond distances (defined as distances between the two heavy atoms forming the hydrogen bond) at the global minima, where double bars represents doubly hydrogen bonded systems; (c) analysis of the components of SAPT energies for the global minimum of the PESs.

to form more favorable hydrogen bonding interactions with hydrogen peroxide than water. Specifically, the dimers containing hydrogen peroxide have more favorable interaction energies by 1.3, 1.1, 1.2, 0.8, 2.2, and 3.3 kcal/mol for methanol, formamide, pyridine-N-oxide, nitromethane, methylamine, and imidazole than the water counterparts. These energy differences predict that sp^3 amine and sp^2 nitrogen functional groups will show the strongest

selectivities for hydrogen peroxide over water interaction. The trend in relative interaction strength between hydrogen peroxide and water-containing heterodimers is generally consistent with the shorter interaction distances between hydrogen peroxide and the model molecules, Figure S2(b). The correlation between the differences of hydrogen bond distances and differences in interaction energies are presented in Fig. S3. Methylamine was found to

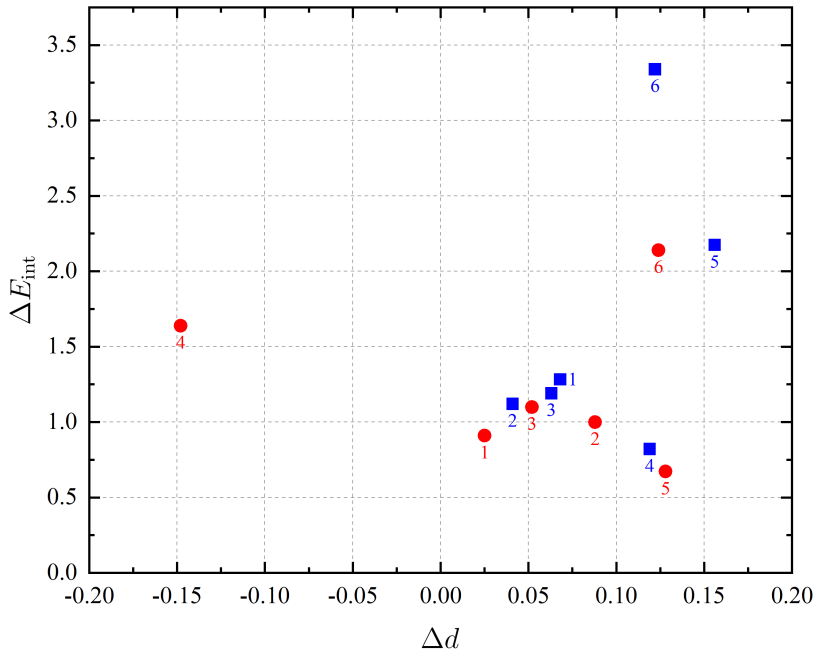

FIG. S3. Correlation between differences of hydrogen bond distances $\Delta d = d_{\mathrm{H_2O}} - d_{\mathrm{H_2O_2}}$ and differences of interaction energies $\Delta E_{\mathrm{int}} = E_{\mathrm{int,H_2O}} - E_{\mathrm{int,H_2O_2}}$. Values for PES minima are in blue and near-experimental geometries are in red. The numbering is as follows: 1 = alcohol, 2 = carbonyl, 3 = *N*-oxide, 4 = nitro, 5 = sp^3, and 6 = sp^2 functional groups.

show the most dramatic difference in hydrogen bonding distance (0.156 Å shorter with hydrogen peroxide) and formamide shows the least difference (0.041 Å shorter with hydrogen peroxide). In all singly-bound (only one hydrogen bond present in the PES minimum geometry) cases, water and hydrogen peroxide are hydrogen bond donors. In the doubly-bound (two hydrogen bonds present in the PES minimum geometry) cases, the shorter and presumably stronger bonds are also of this character. The secondary hydrogen bonds, indicated by sky blue and purple colored bars in Figure S2(b), are donated by the model molecules. The secondary hydrogen bond distances are shorter and therefore presumably stronger for heterodimers containing water.

The components of the interaction energies are shown in Figure S2(c). As the intermolecular distance between monomers shortens, both the attractive and repulsive components increase in magnitude. This relationship explains the correlation between Figure S2(b) and Figure S2(c), i.e., shorter (primary) bonds roughly correlate with larger magnitudes of components. For all dimers, all of the components are larger in magnitude for hydrogen peroxide-containing dimers than for those containing water. For most heterodimers,

the magnitude of the exchange interaction is approximately that of the electrostatic contribution (i.e., the $E^{(1)}_{\rm exch}$ component nearly cancels the $E^{(1)}_{\rm elst}$ component). For this reason, the interaction energy more closely reflects the sum of the induction and dispersion components, emphasizing the importance of including the latter contributions for accurately determining the geometry at the global energy minimum.

VI. COMPARISON OF SAPT AND PES ENERGIES AT NEAR-EXPERIMENTAL GEOMETRIES AND PES GLOBAL MINIMUM GEOMETRIES

Table S15 gives the SAPT and PES interaction energies at the PESs global minimum and at near-experimental geometries, while Table S16 gives the information of PESs developed in this study. In particular, the latter table gives root mean square errors (RMSEs) of the PESs for $E_{\rm int} < 0$. As seen in Table S15, at the global minimum geometries the fits are very accurate, with deviations much smaller than the RMSEs for $E_{\rm int} < 0$ and all percentage errors smaller than 7.7% (in 83% of cases smaller than 3%). This is expected since the global minimum region is the most sampled and weighted region of the PES. At near-experimental geometries, in 50% of cases the deviations are below RMSEs and in 25% of cases are within 0.3 kcal/mol of RMSEs. There are three cases: both water and hydrogen peroxide interacting with N-oxide and water interacting with N sp^3, where accuracy of the fit is poor, with deviations up to 5 times the RMSE. The existence of the regions in configuration space where accuracy is poor is the effect of using the default setting of autoPES for sampling of dimer configurations, which are chosen to minimize the costs of PES developments. As seen in Table S16, the number of grid points ranges between 382 and 1335, whereas other methods of fitting 6-dimensional surfaces use tens of thousands of grid points. In applications to crystal structure predictions, the initial autoPES fit is improved using the dimer configurations extracted from polymorphs generated using the initial fit. This procedure was not needed here since the PESs were used in a very limited way: only to determine the coordinates of dimers that are not fixed by average experimental geometries given in Table S13. All the interaction energies given in the main text and in the SI are from SAPT(DFT) *ab initio* calculations.

TABLE S15. Comparison of SAPT and PES energies at global minimum and near-experimental geometries. E_{int} and V are defined in main text, Δ = E_{int} - V, and % deviation = $|\Delta/E_{\text{int}}| \times 100\%$.

		E_{int}	V	Δ	% deviation
At global minimum geometries					
O-H$\cdots$O-H (Alcohol)	H_2O	-4.43	-4.35	-0.08	1.8
	H_2O_2	-5.71	-5.81	0.10	1.8
O-H$\cdots$O=C (Amide)	H_2O	-7.72	-7.58	-0.14	1.8
	H_2O_2	-8.84	-8.75	-0.09	1.0
O-H$\cdots$O-N (N-oxide)	H_2O	-7.87	-8.05	0.18	2.3
	H_2O_2	-9.06	-9.15	0.09	1.0
O-H$\cdots$$O_2$-N (Nitro)	H_2O	-4.74	-4.61	-0.13	2.7
	H_2O_2	-5.57	-5.74	0.17	3.1
O-H$\cdots$N (sp^3)	H_2O	-5.57	-5.14	-0.43	7.7
	H_2O_2	-7.74	-7.71	-0.03	0.4
O-H$\cdots$N (sp^2)	H_2O	-6.72	-6.34	-0.38	5.7
	H_2O_2	-10.06	-10.07	0.01	0.1
At near-experimental geometries					
O-H$\cdots$O-H (Alcohol)	H_2O	-2.34	-2.39	0.05	2.1
	H_2O_2	-3.25	-3.61	0.36	11.1
O-H$\cdots$O=C (Amide)	H_2O	-4.29	-4.96	0.67	15.6
	H_2O_2	-5.29	-5.28	-0.01	0.2
O-H$\cdots$O-N (N-oxide)	H_2O	-4.74	-5.85	1.11	23.4
	H_2O_2	-5.83	-7.44	1.61	27.6
O-H$\cdots$$O_2$-N (Nitro)	H_2O	-1.90	-1.89	-0.01	0.5
	H_2O_2	-3.54	-3.39	-0.15	4.2
O-H$\cdots$N (sp^3)	H_2O	-5.90	-4.01	-1.89	32.0
	H_2O_2	-6.57	-7.10	0.53	8.1
O-H$\cdots$N (sp^2)	H_2O	-5.71	-5.63	-0.08	1.4
	H_2O_2	-7.85	-8.66	0.81	10.3

TABLE S16. RMSEs (in kcal/mol) of PESs evaluated at close-range grid points with number of grid points given in parentheses. Here, N_{grid}: total number of grid points, N_{FP}: number of free parameters of the PES, and N_{min}: number of detected minima of the PES.

		N_{grid}	N_{FP}	$N_{\text{grid}}/N_{\text{FP}}$	N_{min}	RMSE ($E_{\text{int}} < 0$)
O-H$\cdots$O-H (Alcohol)	H_2O	382	40	9.6	3	0.27 (166)
	H_2O_2	482	54	8.9	6	0.39 (246)
O-H$\cdots$O=C (Amide)	H_2O	422	40	10.6	2	0.37 (188)
	H_2O_2	845	54	15.7	7	0.39 (305)
O-H$\cdots$O-N (N-oxide)	H_2O	830	76	10.9	6	0.43 (413)
	H_2O_2	1265	128	9.9	17	0.39 (694)
O-H$\cdots$$O_2$-N (Nitro)	H_2O	421	46	9.2	4	0.28 (204)
	H_2O_2	568	62	9.2	4	0.28 (264)
O-H$\cdots$N (sp^3)	H_2O	404	46	8.8	1	0.40 (177)
	H_2O_2	1092	62	17.6	8	0.44 (532)
O-H$\cdots$N (sp^2)	H_2O	674	58	11.6	2	0.50 (313)
	H_2O_2	1334	98	13.6	9	0.64 (697)

[1] M. P. Metz, K. Piszczatowski, and K. Szalewicz. Automatic generation of intermolecular potential energy surfaces. *J. Chem. Theory Comput.*, 12:5895–5919, 2016.

[2] A. J. Stone. *The Theory of Intermolecular Forces*. Clarendon Press, Oxford, second edition, 2013.

[3] B. Jeziorski, R. Moszyński, and K. Szalewicz. Perturbation theory approach to intermolecular potential energy surfaces of van der Waals complexes. *Chem. Rev.*, 94:1887–1930, 1994.

[4] K. T. Tang and J. P. Toennies. An improved simple-model for the van der Waals potential based on universal damping functions for the dispersion coefficients. *J. Chem. Phys.*, 80:3726–3741, 1984.

[5] H. L. Williams and C. F. Chabalowski. Using Kohn-Sham orbitals in symmetry-adapted perturbation theory to investigate intermolecular interactions. *J. Phys. Chem. A*, 105:646–659, 2001.

[6] A. J. Misquitta and K. Szalewicz. Intermolecular forces from asymptotically corrected density functional description of monomers. *Chem. Phys. Lett.*, 357:301–306, 2002.

[7] A. Hesselmann and G. Jansen. First-order intermolecular interaction energies from Kohn-Sham orbitals. *Chem. Phys. Lett.*, 357:464–470, 2002.

[8] A. Hesselmann and G. Jansen. Intermolecular induction and exchange-induction energies from coupled-perturbed Kohn-Sham density functional theory. *Chem. Phys. Lett.*, 362:319–325, 2002.

[9] A. J. Misquitta, B. Jeziorski, and K. Szalewicz. Dispersion energy from density-functional theory description of monomers. *Phys. Rev. Lett.*, 91:033201–(1:4), 2003.

[10] A. Hesselmann and G. Jansen. Intermolecular dispersion energies from time-dependent density functional theory. *Chem. Phys. Lett.*, 367:778–784, 2003.

[11] A. J. Misquitta and K. Szalewicz. Symmetry-adapted perturbation theory calculations of intermolecular forces employing density functional description of monomers. *J. Chem. Phys.*, 122:214109–(1:19), 2005.

[12] A. J. Misquitta, R. Podeszwa, B. Jeziorski, and K. Szalewicz. Intermolecular potentials based on symmetry-adapted perturbation theory including dispersion energies from time-dependent density functional calculations. *J. Chem. Phys.*, 123:214103–(1:14), 2005.

[13] A. Hesselmann, G. Jansen, and M. Schütz. Density-functional theory-symmetry-adapted intermolecular perturbation theory with density fitting: A new efficient method to study intermolecular interaction energies. *J. Chem. Phys.*, 122:014103–(1:17), 2005.

[14] R. Bukowski, R. Podeszwa, and K. Szalewicz. Efficient calculations of coupled Kohn-Sham dynamic susceptibility functions and dispersion energies with density fitting. *Chem. Phys. Lett.*, 414:111–116, 2005.

[15] R. Podeszwa, R. Bukowski, and K. Szalewicz. Density fitting methods in symmetry-adapted perturbation theory based on Kohn-Sham description of monomers. *J. Chem. Theory Comput.*, 2:400–412, 2006.

[16] F. Neese. The ORCA program system. *Wiley Interdisciplinary Reviews: Computational Molecular Science*, 2:73–78, 2012.

[17] F. Neese. An improvement of the resolution of the identity approximation for the formation of the Coulomb matrix. *J. Comp. Chem.*, 24:1740–1747, 2003.

[18] J. P. Perdew, K. Burke, and M. Ernzerhof. Generalized gradient approximation made simple. *Phys. Rev. Lett.*, 77:3865–3868, 1996.

[19] M. Grüning, O. V. Gritsenko, S. J. A. van Gisbergen, and E. J. Baerends. Shape corrections to exchange-correlation potentials by gradient-regulated seamless connection of model potentials for inner and outer region. *J. Chem. Phys.*, 114:652–660, 2001.

[20] W. Cencek and K. Szalewicz. On asymptotic behavior of density functional theory. *J. Chem. Phys.*, 139:024104–(1:27), 2013. Erratum: **140**, 149902 (2014).

[21] R. A. Kendall, T. H. Dunning, Jr., and R. J. Harrison. Electron-affinities of the 1st-row atoms revisited - systematic basis-sets and wave-functions. *J. Chem. Phys.*, 96:6796–6806, 1992.

[22] F. Weigend, A. Köhn, and C. Hättig. Efficient use of the correlation consistent basis sets in resolution of the identity MP2 calculations. *J. Chem. Phys.*, 116:3175–3183, 2002.

[23] H. L. Williams, E. M. Mas, K. Szalewicz, and B. Jeziorski. On the effectiveness of monomer-, dimer-, and bond-centered basis functions in calculations of intermolecular interaction energies. *J. Chem. Phys.*, 103:7374–7391, 1995.

[24] R. Podeszwa, R. Bukowski, and K. Szalewicz. Potential energy surface for the benzene dimer and perturbational analysis of $\pi - \pi$ interactions. *J. Phys. Chem. A*, 110:10345–10354, 2006.

[25] R. Bukowski, W. Cencek, P. Jankowski, M. Jeziorska, B. Jeziorski, S. A. Kucharski, V. F. Lotrich, M. P. Metz, A. J. Misquitta, R. Moszyński, K. Patkowski, R. Podeszwa, F. Rob, S. Rybak, K. Szalewicz, H. L. Williams, R. J. Wheatley, P. E. S. Wormer, and P. S. Żuchowski. SAPT2016: An *ab initio* program for many-body symmetry-adapted perturbation theory calculations of intermolecular interaction energies. University of Delaware and University of Warsaw, 2016.

[26] M. Jeziorska, B. Jeziorski, and J. Cizek. Direct calculation of the Hartree-Fock interaction energy via exchange perturbation expansion - the He–He interaction. *Int. J. Quantum Chem.*, 32:149–164, 1987.

[27] K. Patkowski, K. Szalewicz, and B. Jeziorski. Third-order interactions in symmetry-adapted perturbation theory. *J. Chem. Phys.*, 125:154107–(1:20), 2006.

[28] R. Podeszwa, W. Cencek, and K. Szalewicz. Efficient calculations of dispersion energies for nanoscale systems from coupled density response functions. *J. Chem. Theory Comput.*, 8:1963–1969, 2012.